LETTER

doi:10.1038/nature24631

Rotation in [C II]-emitting gas in two galaxies at a redshift of 6.8

Renske Smit[1,2], Rychard J. Bouwens[3], Stefano Carniani[1,2], Pascal A. Oesch[4], Ivo Labbé[3], Garth D. Illingworth[5], Paul van der Werf[3], Larry D. Bradley[6], Valentino Gonzalez[7,8], Jacqueline A. Hodge[3], Benne W. Holwerda[9], Roberto Maiolino[1,2] & Wei Zheng[10]

The earliest galaxies are thought to have emerged during the first billion years of cosmic history, initiating the ionization of the neutral hydrogen that pervaded the Universe at this time. Studying this 'epoch of reionization' involves looking for the spectral signatures of ancient galaxies that are, owing to the expansion of the Universe, now very distant from Earth and therefore exhibit large redshifts. However, finding these spectral fingerprints is challenging. One spectral characteristic of ancient and distant galaxies is strong hydrogen-emission lines (known as Lyman-α lines), but the neutral intergalactic medium that was present early in the epoch of reionization scatters such Lyman-α photons. Another potential spectral identifier is the line at wavelength 157.4 micrometres of the singly ionized state of carbon (the [C II] $\lambda = 157.74\,\mu$m line), which signifies cooling gas and is expected to have been bright in the early Universe. However, so far Lyman-α-emitting galaxies from the epoch of reionization have demonstrated much fainter [C II] luminosities than would be expected from local scaling relations[1–5], and searches for the [C II] line in sources without Lyman-α emission but with photometric redshifts greater than 6 (corresponding to the first billion years of the Universe) have been unsuccessful. Here we identify [C II] $\lambda = 157.74\,\mu$m emission from two sources that we selected as high-redshift candidates on the basis of near-infrared photometry; we confirm that these sources are two galaxies at redshifts of $z = 6.8540 \pm 0.0003$ and $z = 6.8076 \pm 0.0002$. Notably, the luminosity of the [C II] line from these galaxies is higher than that found previously in star-forming galaxies with redshifts greater than 6.5. The luminous and extended [C II] lines reveal clear velocity gradients that, if interpreted as rotation, would indicate that these galaxies have similar dynamic properties to the turbulent yet rotation-dominated disks that have been observed in Hα-emitting galaxies two billion years later, at 'cosmic noon'.

Using the Atacama Large Millimetre Array (ALMA) in Chile, we obtained spectroscopy at 241–245 GHz for two Lyman-break galaxies (LBGs)—COS-3018555981 and COS-2987030247—at an estimated photometric redshift of just less than 7, corresponding to roughly 800 million years after the Big Bang. These two sources are luminous in the rest-frame ultraviolet (UV; $L_{\rm UV}$ is roughly $2 \times L^*_{z=7}$ (this latter value being obtained from ref. 6)), but are representative of 'normal' star-forming galaxies at redshifts of around 7, with a UV-based star-formation rate (SFR) of (19–23)$M_\odot\ {\rm yr}^{-1}$ (L, luminosity; $M_\odot$, mass of the Sun). We selected these sources on the basis of the blue rest-frame optical colours measured in the 3.6-μm and 4.5-μm photometric bands by the Spitzer Space Telescope[7]; these rest-frame colours strongly constrain the photometric redshift probability distribution to the range $6.6 < z < 6.9$. The two sources are among the most extreme [O III] + Hβ emitters known at redshifts of around 7 (refs 7, 8). We observed them using a 36-antennae ALMA configuration (angular resolution $1.1'' \times 0.7''$, equivalent to 5.8 kpc × 3.7 kpc at $z = 6.8$), with 24 minutes of source-integration time for each target. Using this spectral scan, we searched for [C II] lines in the redshift range $z_{\rm [C\,II]} = 6.74$–6.90. Our results are summarized in Extended Data Table 1.

We detected a line at 241.97 ± 0.01 GHz and at 243.42 ± 0.01 GHz for COS-3018555981 and COS-2987030247, respectively, in both one-dimensional spectra and spectral-line-averaged maps (Fig. 1; more than 5σ significance). We thereby derived spectroscopic redshifts of $z_{\rm [C\,II]} = 6.8540 \pm 0.0003$ and $z_{\rm [C\,II]} = 6.8076 \pm 0.0002$, respectively, in excellent agreement with the photometric redshift estimates of 6.76 ± 0.07 and 6.66 ± 0.14 for COS-3018555981 and COS-2987030247; we also derived line-widths of $232 \pm 30\,{\rm km}^{-1}$ and $124 \pm 18\,{\rm km}^{-1}$, respectively. Although successful line searches have previously confirmed far-infrared lines in submillimetre-selected star-bursting galaxies at redshifts of more than 6 (refs 9, 10), and a few tantalizing 'blind' candidate [C II] emitters (with no optical or near-infrared counterpart) have been detected with a significance of around 4σ (ref. 11), this is the first time that normal star-forming galaxies in this early epoch—selected at optical or near-infrared wavelengths—have confidently been spectroscopically confirmed with ALMA.

We furthermore obtained upper limits to the far-infrared dust-continuum emission from the ALMA data. We found infrared SFRs of less than (16–19)$M_\odot\ {\rm yr}^{-1}$—rates that are consistent with 'normal' star-forming galaxies in the local Universe[12], and which rule out the presence of a dusty starburst in these sources. Figure 2 shows that, given the colour of the UV-continuum slopes of these sources (this slope, $\beta_{\rm UV}$, is roughly −1.2), a higher dust content (measured by the infrared excess, $L_{\rm IR}/L_{\rm UV}$) would be expected if the sources obeyed the Meurer dust law, which is observed to apply for local starburst galaxies[13]. Scatter in the IRX–$\beta_{\rm UV}$ relation could be due to the geometry of the dust, the age of the population of galaxies, or the shape of the attenuation curve. However, for blue galaxies (where $\beta_{\rm UV}$ is less than around −0.5) that scatter below the Meurer[13] relation—such as our selected galaxies—the most likely way to reproduce the low observed values of IRX is through a steeper attenuation curve, such as that derived for the Small Magellanic Cloud[14] (consistent with our measurements to within 3σ), in combination with a potential increase in dust temperature at higher redshifts.

In Fig. 2 we present the measured flux of the [C II] lines as a function of the SFR, which is consistent with the SFR–$L_{\rm [C\,II]}$ relation for galaxies in the local Universe (ref. 15), and consistent with data for similarly bright galaxies observed at redshifts of about 5–6 (refs 16, 17). By contrast, [C II] observations from the epoch of reionization so far have shown

[1]Cavendish Laboratory, University of Cambridge, 19 JJ Thomson Avenue, Cambridge CB3 0HE, UK. [2]Kavli Institute for Cosmology, University of Cambridge, Madingley Road, Cambridge CB3 0HA, UK. [3]Leiden Observatory, Leiden University, NL-2300 RA Leiden, Netherlands. [4]Observatoire de Genève, Université de Genève, Chemin des Maillettes 51, CH-1290 Versoix, Switzerland. [5]UCO/Lick Observatory, University of California, Santa Cruz, 1156 High Street, Santa Cruz, California 95064, USA. [6]Space Telescope Science Institute, 3700 San Martin Drive, Baltimore, Maryland 21218, USA. [7]Departmento de Astronomia, Universidad de Chile, Casilla 36-D, Santiago 7591245, Chile. [8]Centro de Astrofisica y Tecnologias Afines (CATA), Camino del Observatorio 1515, Las Condes, Santiago 7591245, Chile. [9]Department of Physics and Astronomy, University of Louisville, Louisville, Kentucky 40292, USA. [10]Department of Physics and Astronomy, The Johns Hopkins University, 3400 North Charles Street, Baltimore, Maryland 21218, USA.

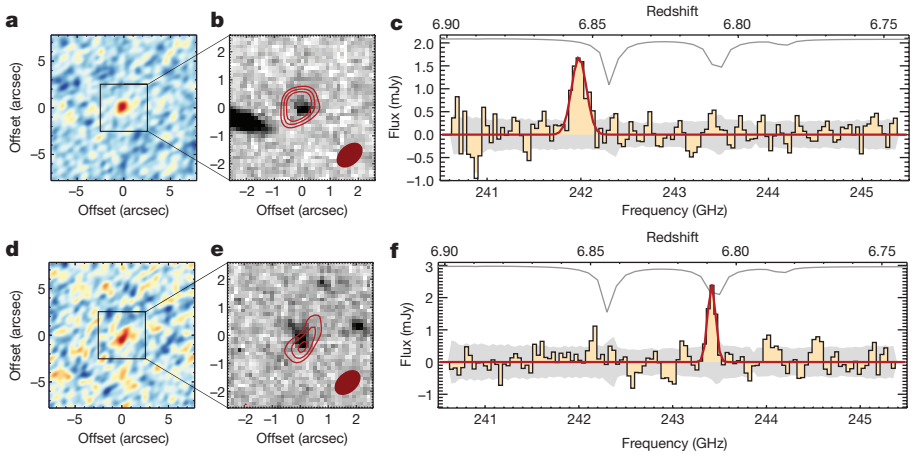

Figure 1 | Spectroscopic line confirmations of the galaxies targeted in this study. ALMA line maps and spectra for two galaxies with photometric redshifts (z_{phot}) in the range $6.6 < z_{phot} < 6.9$ (ref. 7). We detect a 8.2σ [C II] line at $z_{[C\,II]} = 6.8540 \pm 0.0003$ in galaxy COS-3018555981 (**a**–**c**), and a roughly 5.1σ [C II] line at $z_{[C\,II]} = 6.8076 \pm 0.0002$ in galaxy COS-2987030247 (**d**–**f**). **a**, **d**, $20'' \times 20''$ images of the ALMA cube (before primary-beam correction), collapsed over 241.85–242.10 GHz for COS-3018555981 and 243.35–243.45 GHz for COS-2987030247 (with root-mean-squares of 0.1 mJy and 0.2 mJy, respectively). **b**, **e**, $5'' \times 5''$ images of the targeted sources. Hubble Space Telescope H_{160}-band imaging is shown in greyscale; the overlaid red contours show the 3σ, 4σ and 5σ levels of the spectral-line-averaged maps on the left. The filled ellipses in the bottom right corners indicate the beam size ($1.1'' \times 0.7''$ half-power widths). **c**, **f**, The spectra extracted from within a contour of the half-maximum power in the line maps. The red lines show the best-fitting Gaussian line profiles; the grey lines at the top show the atmospheric absorption; the grey filled regions give the $\pm 1\sigma$ noise in the spectrum.

that these galaxies fall substantially below the local relation[1–5]. This is probably because we chose our $z > 6.5$ targets differently to previous authors: we selected [O III] + Hβ emitters as opposed to Lyman-α-emitting galaxies.

Our sources have slightly higher SFRs and redder UV slopes (at roughly −1.2) than previously studied galaxies from this epoch, which could indicate that our galaxies are more evolved and more metal rich. Sources with extremely low oxygen abundance in the local Universe are typically found to be [C II] deficient[15,18] owing to their hard radiation field, and therefore metallicity could be an important discriminator between [C II]-bright and [C II]-faint sources[19]. Moreover, in local galaxies the SFR surface density (Σ_{SFR}) drives a continuous trend of deepening [C II] deficit as a function of increasing Σ_{SFR} (refs 18, 20), indicating that local processes such as the radiation-field intensity are important in driving [C II] luminosity. If [C II]-faint sources at $z > 6$, currently unresolved in [C II] lines, have higher star-formation surface brightness than our galaxies, this could also explain the different SFR/$L_{[C\,II]}$ ratios.

Furthermore, our sources have high-equivalent-width optical emission lines, which could suggest an ongoing starburst and potentially a higher fraction of [C II] emission emerging from H II regions. Starbursts and H II galaxies in the local Universe have slightly elevated [C II] luminosities for a given SFR[15], and therefore we could specifically be targeting the brightest [C II] galaxies of the overall $z \approx 7$ galaxy population. Finally, while we do not have spectroscopy covering the Lyman-α line for COS-3018555981 and COS-2987030247, our sources could be weaker Lyman-α emitters than are typically seen in spectroscopically confirmed sources at this redshift. Lyman-α emission is suggested to be inversely correlated with neutral gas column density[21] and can therefore affect the visibility of [C II], which emerges both in the diffuse neutral and in the warm ionized medium of a galaxy.

We also determined [C II] half-light radii (deconvolved from the beam size) of 2.6 ± 0.8 kpc and 3.1 ± 1.0 kpc for COS-3018555981 and COS-2987030247—nearly twice the half-light radius of the UV in the brightest LBGs at this redshift[22]. We used the spatial extent of the [C II] detection to investigate the velocity structure of these sources, which reveals a projected velocity difference over the galaxy of 111 ± 28 km s^{-1} and 54 ± 20 km s^{-1} for COS-3018555981 and COS-2987030247, respectively (Fig. 3), similar to the velocity gradients observed recently in two galaxies at redshifts of around 5–6 (refs 23, 24). Given the low angular resolution of the observations, there are various ways to interpret these velocity gradients. A rotating galaxy disk would be one interpretation; however, a merger involving one or more [C II]-emitting galaxies, smoothed by the beam size, could also appear as a regular rotational field. Furthermore, a bipolar outflow or perhaps an inflow of gas could provide an additional velocity component to the [C II] line that might give the impression of galaxy rotation.

We applied an observational criterion for the classification of rotation- and dispersion-dominated systems, based on the full observed velocity gradient, Δv_{obs}, and the integrated line width, σ_{tot}, of a galaxy, such that $\Delta v_{obs}/2\sigma_{tot}$ values of more than 0.4 are likely to be rotation-dominated sources[25]. In Fig. 4, we compare this quantity for

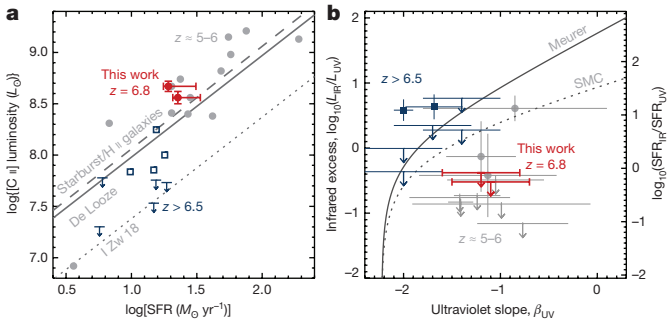

Figure 2 | [C II] luminosity and dust continuum for $z > 5$ galaxies. **a**, [C II] line luminosity as a function of the SFR for COS-3018555981 and COS-2987030247 (red points; error bars for the SFRs reflect 1σ upper limits on the infrared continuum), compared with [C II] detections at redshifts of around 5–6 (light grey points)[4,16,17] and more than 6.5 (blue open squares and arrows)[1–3,5]. Locally observed relations[15] are indicated by solid lines (star-forming galaxies) and dashed lines (starburst and H II galaxies). The dotted line gives the 0.6-dex offset from the local relation found for the dwarf galaxy I Zwicky 18 ('I Zw 18'). **b**, Infrared excess (L_{UV}/L_{IR}) as a function of the UV-continuum slope (β_{UV}) of our sources compared with expectations from the Meurer[13] relation (solid grey line) and a similar relation based on the dust law of the Small Magellanic Cloud[14] (SMC; dotted grey line). We include [C II] detections at redshifts of around 5–6 as light grey points[16], and detections (and upper limits) at redshifts greater than 6.5 as blue solid squares (and arrows)[28–30]. Upper limits and error bars represent 1σ significance levels. $L_{\odot}$, luminosity of the Sun.

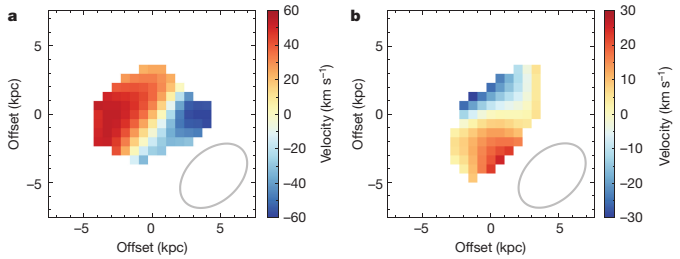

Figure 3 | Velocity structure of the detected [C II] emission in COS-3018555981 and COS-2987030247. a, **b**, Velocity fields measured in COS-3018555981 (**a**) and COS-2987030247 (**b**). The observations are spatially resolved, as shown by the beam size of the observations (grey ellipses), and reveal a projected velocity difference over the galaxies of $111 \pm 28\,\mathrm{km^{-1}}$ and $54 \pm 20\,\mathrm{km^{-1}}$, respectively. Given the low angular resolution of the observations, we could interpret the velocity gradients as disk rotation or alternatively perhaps as a merging system with two or more velocity components.

our galaxies with that measured through Hα emission for galaxies at redshifts of around 1 to 3 (ref. 25). Although our sources are an order of magnitude smaller in terms of stellar mass, and at an epoch 2.5 billion years earlier in cosmic time, we find $\Delta v_{\mathrm{obs}}/2\sigma_{\mathrm{tot}}$ values of 0.57 ± 0.16 and 0.52 ± 0.21 for COS-3018555981 and COS-2987030247—similar to the values for the turbulent yet rotationally supported galaxy disks at redshifts of about 2 (ref. 25). Assuming a circularly symmetric galaxy disk model, we estimate dynamic masses, M_{dyn}, of $1.0^{+0.3}_{-0.2} \times 10^{10} M_{\odot}$ and $0.4^{+0.9}_{-0.3} \times 10^{10} M_{\odot}$ for COS-3018555981 and COS-2987030247, respectively. (Note, however, that the influence of turbulence in these sources could increase the dynamic mass estimates, although by at most a factor of two.) Therefore, these sources have around four to ten times less mass than the bright, UV-selected sources observed recently at redshifts of around 5 to 6 (corresponding to just 200–300 million years later in cosmic time[16]), which otherwise appear similar in their [C II] and infrared properties (Fig. 2). Furthermore, the stellar mass in our sources makes up about 14% and 43% of the total dynamic mass that we measure (Fig. 4), in good

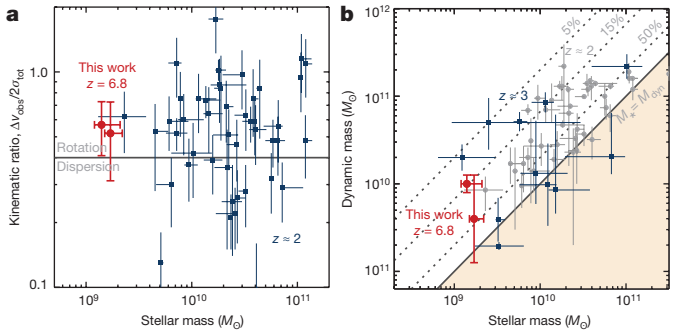

Figure 4 | Dynamic classification and masses of galaxies with redshifts of around 2 or more. a, The observed kinematic ratio of the projected velocity range of a galaxy over the velocity dispersion of the system ($\Delta v_{\mathrm{obs}}/2\sigma_{\mathrm{tot}}$) as a function of stellar mass, for COS-3018555981 and COS-2987030247 (red points), and for Hα-emitting galaxies from the SINS[25] spectroscopy survey at redshifts of about 2 (blue squares). Galaxies with $\Delta v_{\mathrm{obs}}/2\sigma_{\mathrm{tot}}$ ratios of more than 0.4 are classified as probable rotation-dominated systems, while sources with $\Delta v_{\mathrm{obs}}/2\sigma_{\mathrm{tot}}$ ratios of less than 0.4 are probably dispersion-dominated (demarcated by the grey line)[25]. **b**, Dynamic (total) mass within a roughly 2-kpc half-light radius (assuming a circularly symmetric thin-disk model) is plotted against stellar mass for our sources (red points). Grey dotted lines indicate stellar mass as a fraction of total dynamic mass; the stellar-mass fractions of 14% and 43% for COS-3018555981 and COS-2987030247 are in good agreement with the range of values found for galaxies in the AMAZE survey[26] at redshifts of about 3 (blue squares) and in the SINS survey[25] for redshifts of about 2 (grey points). Error bars represent 1σ.

agreement with the 33% stellar mass estimated for the UV-selected sources at redshifts of about 5–6 (ref. 16), and consistent with the wide range of values observed for star-forming galaxies at redshifts of around 1–3 (refs 25, 26). These results indicate a substantial gas fraction in the inner few kiloparsecs of our galaxies, consistent with hydrodynamic simulations of star-forming galaxies at this epoch[27].

Online Content Methods, along with any additional Extended Data display items and Source Data, are available in the online version of the paper; references unique to these sections appear only in the online paper.

Received 15 June; accepted 3 October 2017.

1. Ouchi, M. *et al.* An intensely star-forming galaxy at $z \sim 7$ with low dust and metal content revealed by deep ALMA and HST observations. *Astrophys. J.* **778,** 102 (2013).
2. Ota, K. *et al.* ALMA observation of 158 [C II] line and dust continuum of a $z = 7$ normally star-forming galaxy in the epoch of reionization. *Astrophys. J.* **792,** 34 (2014).
3. Maiolino, R. *et al.* The assembly of 'normal' galaxies at $z \sim 7$ probed by ALMA. *Mon. Not. R. Astron. Soc.* **452,** 54–68 (2015).
4. Knudsen, K. K. *et al.* [C II] emission in $z \sim 6$ strongly lensed, star-forming galaxies. *Mon. Not. R. Astron. Soc.* **462,** L6–L10 (2016).
5. Pentericci, L. *et al.* Tracing the reionization epoch with ALMA: [C II] emission in $z \sim 7$ galaxies. *Astrophys. J.* **829,** L11 (2016).
6. Stark, D. P. Galaxies in the first billion years after the Big Bang. *Annu. Rev. Astron. Astrophys.* **54,** 761–803 (2016).
7. Smit, R. *et al.* High-precision photometric redshifts from Spitzer/IRAC: extreme [3.6]–[4.5] colors identify galaxies in the redshift range $z \sim 6.6$–6.9. *Astrophys. J.* **801,** 122 (2015).
8. Smit, R. *et al.* Evidence for ubiquitous high-equivalent-width nebular emission in $z \sim 7$ galaxies: toward a clean measurement of the specific star-formation rate using a sample of bright, magnified galaxies. *Astrophys. J.* **784,** 58 (2014).
9. Riechers, D. A. *et al.* A dust-obscured massive maximum-starburst galaxy at a redshift of 6.34. *Nature* **496,** 329–333 (2013).
10. Strandet, M. L. *et al.* ISM properties of a massive dusty star-forming galaxy discovered at $z \sim 7$. *Astrophys. J.* **842,** L15 (2017).
11. Aravena, M. *et al.* The ALMA spectroscopic survey in the Hubble ultra deep field: search for [CII] line and dust emission in $6 < z < 8$ galaxies. *Astrophys. J.* **833,** 71 (2016).
12. Leroy, A. K. *et al.* Estimating the star formation rate at 1 kpc scales in nearby galaxies. *Astron. J.* **144,** 3 (2012).
13. Meurer, G. R., Heckman, T. M. & Calzetti, D. Dust absorption and the ultraviolet luminosity density at $z \sim 3$ as calibrated by local starburst galaxies. *Astrophys. J.* **521,** 64–80 (1999).
14. Prevot, M. L., Lequeux, J., Prevot, L., Maurice, E. & Rocca-Volmerange, B. The typical interstellar extinction in the Small Magellanic Cloud. *Astron. Astrophys.* **132,** 389–392 (1984).
15. De Looze, I. *et al.* The applicability of far-infrared fine-structure lines as star formation rate tracers over wide ranges of metallicities and galaxy types. *Astron. Astrophys.* **568,** A62 (2014).
16. Capak, P. L. *et al.* Galaxies at redshifts 5 to 6 with systematically low dust content and high [C II] emission. *Nature* **522,** 455–458 (2015).
17. Willott, C. J., Carilli, C. L., Wagg, J. & Wang, R. Star formation and the interstellar medium in $z > 6$ UV-luminous Lyman-break galaxies. *Astrophys. J.* **807,** 180 (2015).
18. Smith, J. D. T. *et al.* The spatially resolved [CII] cooling line deficit in galaxies. *Astrophys. J.* **834,** 5 (2017).
19. Vallini, L., Ferrara, A., Pallottini, A. & Gallerani, S. Molecular cloud photoevaporation and far-infrared line emission. *Mon. Not. R. Astron. Soc.* **467,** 1300–1312 (2017).
20. Herrera-Camus, R. *et al.* [C II] 158 μm emission as a star formation tracer. *Astrophys. J.* **800,** 1 (2015).
21. Stark, D. P. *et al.* Lyα and C III] emission in $z = 7$–9 galaxies: accelerated reionization around luminous star-forming systems? *Mon. Not. R. Astron. Soc.* **464,** 469–479 (2017).
22. Bowler, R. A. A., Dunlop, J. S., McLure, R. J. & McLeod, D. J. Unveiling the nature of bright $z \sim 7$ galaxies with the Hubble Space Telescope. *Mon. Not. R. Astron. Soc.* **466,** 3612–3635 (2017).
23. Riechers, D. A. *et al.* ALMA imaging of gas and dust in a galaxy protocluster at redshift 5.3: [C II] emission in "typical" galaxies and dusty starbursts ~1 billion years after the Big Bang. *Astrophys. J.* **796,** 84 (2014).
24. Pavesi, R. *et al.* ALMA reveals weak [N II] emission in "typical" galaxies and intense starbursts at $z = 5$–6. *Astrophys. J.* **832,** 151 (2016).
25. Förster Schreiber, N. M. *et al.* The SINS survey: SINFONI integral field spectroscopy of $z \sim 2$ star-forming galaxies. *Astrophys. J.* **706,** 1364–1428 (2009).
26. Gnerucci, A. *et al.* Dynamical properties of AMAZE and LSD galaxies from gas kinematics and the Tully–Fisher relation at $z \sim 3$. *Astron. Astrophys.* **528,** A88 (2011).
27. Fiacconi, D. *et al.* Young and turbulent: the early life of massive galaxy progenitors. *Mon. Not. R. Astron. Soc.* **467,** 4080–4100 (2017).

28. Watson, D. *et al.* A dusty, normal galaxy in the epoch of reionization. *Nature* **519,** 327–330 (2015).
29. Schaerer, D. *et al.* New constraints on dust emission and UV attenuation of $z = 6.5–7.5$ galaxies from millimeter observations. *Astron. Astrophys.* **574,** A19 (2015).
30. Laporte, N. *et al.* Dust in the reionization era: ALMA observations of a $z = 8.38$ gravitationally lensed galaxy. *Astrophys. J.* **837,** L21 (2017).

Acknowledgements This paper makes use of the following ALMA data: ADS/JAO.ALMA#2015.1.01111.S (http://almascience.org/aq?project_code=2015.1.01111.S). ALMA is a partnership of the European Southern Observatory (ESO, UK), the National Science Foundation (NSF, USA) and the National Institute of Natural Sciences (NINS, Japan), together with the National Research Council (NRC, Canada), the National Security Council (NSC) and Academia Sinica Institute of Astronomy and Astrophysics (ASIAA, Taiwan), and the Korea Astronomy and Space Science Institute (KASI, South Korea), in cooperation with Chile. The Joint ALMA Observatory is operated by ESO, Associated Universities Inc. (AUI)/National Radio Astronomy Observatory (NRAO), and the National Astronomical Observatory of Japan (NAOJ). This work is part of a Rubicon programme, 'A multi-wavelength view of the first galaxies', with project number 680-50-1518, which is financed by the Netherlands Organisation for Scientific Research (NWO). R.M. and S.C. acknowledge ERC Advanced Grant 695671 'QUENCH' and support by the Science and Technology Facilities Council (STFC).

Author Contributions R.S. performed the data reduction and nearly all data analysis for this work. S.C. carried out the modelling of a thin disk to the velocity fields. R.S. led the telescope proposal to obtain the dataset, with a number of key ideas contributed by R.J.B. R.S. was responsible for making all of the figures and writing most of the text. R.J.B., S.C., P.A.O., I.L., G.D.I., P.v.d.W., L.D.B., V.G., J.A.H., B.W.H., R.M. and W.Z. contributed feedback on the various versions of this manuscript and on the telescope proposal.

Author Information Reprints and permissions information is available at www.nature.com/reprints. The authors declare no competing financial interests. Readers are welcome to comment on the online version of the paper. Publisher's note: Springer Nature remains neutral with regard to jurisdictional claims in published maps and institutional affiliations. Correspondence and requests for materials should be addressed to R.S. (rs940@cam.ac.uk).

METHODS

Definitions. Throughout this paper we adopt a Chabrier[31] initial mass function (IMF). For ease of comparison with previous studies, we take H_0 (the Hubble constant) to be 70 km s^{-1} Mpc^{-1}, Ω_m (the matter density) to be 0.3, and Ω_Λ (the dark-energy density) to be 0.7, which gives a physical scale of 5.3 kpc per pixel at $z = 6.8$. Magnitudes are quoted in the AB system[32]. Units are given in terms of solar mass (where $M_\odot = 1.99 \times 10^{33}$ g) and solar luminosity (where $L_\odot = 3.84 \times 10^{33}$ erg s^{-1}) where possible.

Data. We obtained ALMA observations centred on the sources COS-3018555981 (right ascension (RA) = 10 h 30 min 185 s; declination (dec.) = +02° 15′ 59.81″) and COS-2987030247 (RA = 10 h 0 min 29.870 s; dec. = +02° 13′ 02.47″) as part of a filler programme (project code 2015.1.01111.S; principal investigator R.S.) on 14 April 2016, in cycle 3. We requested three tunings to cover the frequency range 1,870.74–1,971.43 GHz in band 6, in order to scan for [C II] at redshift $z = 6.45$–6.90, corresponding to the 99% photometric redshift probability range[7]. One tuning was executed, scanning the redshift range $z_{[C\,II]} = 6.74$–6.90, with 24 min of source-integration time for each of the targets. The precipitable water vapour (PWV) of the observations was 1.34 mm. The array consisted of 36 antennas and three spectral windows having a bandwidth of 1.875 GHz, to cover a frequency range of 4.95 GHz in a single sideband.

We calibrated and reduced the data with Common Astronomy Software Application (CASA)[33] version 4.5.3, using the automated pipeline, and we imaged the data with the CLEAN task (requiring no iterations, as no continuum sources are detected in the data), using a natural weighting for optimal signal-to-noise. The resulting observations reached an image root-mean-square (r.m.s.) sensitivity of 0.32 mJy beam^{-1} at 243 GHz in a 50 km s^{-1} channel in both pointings. The primary beam has a resolution of 1.1″ × 0.7″ (position angle −48°) for both targets.

We also made use of Hubble Space Telescope (HST) WFC3/F160W (H_{160}) imaging, as well as the photometry of these objects that was used in the selection of our galaxies previously[7].

Line detections. *COS-3018555981.* We extracted a spectrum from the ALMA cube that was centred on the rest-frame UV continuum of the galaxy detected in the HST H_{160} band of COS-3018555981 as a first guess, and found a clear line detected at around 242 GHz, removed from any atmospheric absorption features and with a peak flux of more than 3.5σ above the local noise. Next, we extracted a spectrally averaged map between 241.85 GHz and 242.10 GHz; this map revealed that the emission line was centred on a faint wing of the UV-continuum detection, 0.27″ removed from the brightest UV clump (Fig. 1). This offset is similar to the typical uncertainty in the HST astrometry of 0.2″ (ref. 34); however, if instead the offset is real, this could quite reasonably suggest that the brightest star-forming region in the UV does not spatially coincide with the dynamic centre of the system.

We determined the significance of the detection by measuring the flux on the spectral-line-averaged map in a 1.1″ × 0.7″ aperture corresponding to the full-width at half-maximum (FWHM) of the beam, and we repeated this measurement 9,000 times at randomly selected positions of the image, resulting in an estimated signal-to-noise ratio of 8.2. To determine the redshift of COS-3018555981, we extracted a new one-dimensional spectrum from all pixels above the half-maximum of the line detection on the spectral-line-averaged map, and we fitted a Gaussian to the observed line to determine a line centre of 241.97 ± 0.01 GHz, corresponding to a [C II] redshift of 6.8540 ± 0.0003, and a linewidth of 232 ± 30 km^{-1} FWHM (Fig. 1). The only lines other than [C II] $\lambda = 158\,\mu$m that are expected to be bright enough to be able to explain our detection are [O I] $\lambda = 63\,\mu$m and [O III] $\lambda = 88\,\mu$m. However, the [O I] $\lambda = 63\,\mu$m and [O III] $\lambda = 88\,\mu$m redshifts of 18.6 and 13.02, respectively, are inconsistent with the HST photometry for this source[7]. Furthermore, the photometric redshift of 6.76 ± 0.07 (ref. 7) is also inconsistent with the [O I] $\lambda = 145\,\mu$m redshift of 7.5, which is the closest infrared line in frequency, if many times fainter, to [C II] $\lambda = 158\,\mu$m.

COS-2987030247. Similarly to the procedure for COS-3018555981, we first searched for an emission line in the spectrum extracted over the rest-frame UV continuum of COS-2987030247. We found a tentative narrow line at 243.4 GHz—40 MHz removed from an atmospheric absorption feature at 243.5 GHz, where the r.m.s. is 1.5 times greater than the median r.m.s. in the data cube. The spectral-line-averaged map extracted between 243.35 GHz and 243.45 GHz shows a >5σ detection close to the position of the HST counterpart; that is, the peak of the map is 0.17″ removed from the UV-continuum emission (Fig. 1).

By sampling the noise in the spectral-line-averaged map in ellipsoidal apertures of the beam size, we measured a signal-to-noise ratio of 5.1 for the detected line at 243.5 GHz, suggesting that the line is indeed a real detection. To further test the significance of the line we performed a blind line search of the data cube. For each pixel in the cube we extracted a one-dimensional spectrum from averaging all pixels within the ellipsoidal aperture of the beam size, and we fitted any tentative lines in the spectrum with a Gaussian. If the difference between the χ^2 of the line fit and that of a straight line was greater than 25 (that is, 5σ), we extracted a velocity-averaged image over the FWHM of the line and inspected the significance of the detection on this image. To remove spurious line detections, we again assessed the significance of any potential line from the random sampling of the flux in ellipsoidal apertures on the line map. While we robustly detected the line over COS-2987030247, we found no other sources with a >5σ detection in both the one-dimensional spectrum and the spectral-line-averaged map. This test, in combination with the small spatial offset from our HST target, confirms that our line detection over COS-2987030247 is real, and not due to a spurious detection showing up close to the r.m.s. peak of the atmospheric absorption feature.

We extracted a new spectrum from all pixels with a flux above the half-maximum flux in the spectral-line-averaged map, and used this to measure a spectroscopic redshift of $z_{[C\,II]} = 6.8076 \pm 0.0002$ for COS-2987030247, in good agreement with the photometric redshift of $z_{phot} = 6.66 \pm 0.14$.

Dust. We obtained dust continuum measurements after identifying the [C II] line in our data, by averaging the remaining part of the data cubes in frequency. We did not find any evidence for flux above the 1σ noise level in the mean continuum image at the source positions. Therefore, we put an upper limit on the continuum flux, and assumed a grey-body approximation for the dust continuum by considering a range of infrared slopes where we varied both the slope (in the range $\beta_{IR} = 1$–2) and the dust temperature (in the range $T_{dust} = 20$–60 K). We derived a 3σ upper limit on the infrared luminosity of $1.3 \times 10^{11} L_\odot$ and $1.1 \times 10^{11} L_\odot$ for COS-3018555981 and COS-2987030247, respectively.

Given that the UV continuum of galaxies is substantially attenuated by even small amounts of dust, comparing the UV colour and the infrared excess—IRX = L_{UV}/L_{IR}—can provide insights into the dust-attenuation curve in these galaxies. We derived the UV-continuum slope β_{UV}, where the flux density is $f_\lambda \propto \lambda^{\beta_{UV}}$, from a power-law fit to the HST J_{125} and H_{160} photometry; we found values of -1.22 ± 0.51 and -1.18 ± 0.53 for COS-3018555981 and COS-2987030247, respectively. Often, interpreting the infrared excess as a means to constrain the dust-attenuation curve can be affected by the geometry of the dust[35]. In particular, a spatial offset between dust-obscured star-forming regions and unobscured UV-emitting regions can produce bluer UV colours for a given IRX[36]. The small spatial offsets measured between the UV continuum and [C II] emission in our sources might indicate such an effect of dust geometry here. However, given that our sources already appear much redder than would be predicted by the Meurer[13] relation for a given IRX, our conclusions are not affected by any spatial offsets of the dust continuum with respect to the UV light.

Star-formation rate and stellar mass. We obtained constraints on the UV-based SFRs rates from the J_{125} band photometry (corresponding to the rest-frame at around 1,600 Å), and on the infrared-based SFRs from the upper limits on the infrared luminosity, and we converted from luminosity to SFRs using the Kennicutt[37] scaling relations. For COS-3018555981, a foreground object of $z = 0.74$ is visible at a projected distance of 2.6″, which could introduce a small boost to the measured fluxes owing to gravitational lensing. However, the stellar mass of this object is only $4 \times 10^9 M_\odot$ (ref. 38), which suggests a modest halo mass, and therefore we estimate the magnification of this source to be no more than 0.1 magnitude (that is, no larger than the measured random errors), as discussed recently[22].

Using the deconvolved size of the [C II] emission as the size of the galaxy, we found a SFR density, Σ_{SFR}, of $0.91 M_\odot$ yr^{-1} kpc^{-2} and $0.75 M_\odot$ yr^{-1} kpc^{-2} for COS-3018555981 and COS-2987030247, respectively. This is in good agreement with the SFRs obtained using [C II] as a spatially resolved SFR indicator, using the relation calibrated for galaxies from the local KINGFISH sample[20], which predicts a Σ_{SFR} of $0.68 M_\odot$ yr^{-1} kpc^{-2} and $0.34 M_\odot$ yr^{-1} kpc^{-2} on the basis of the [C II] surface brightness, $\Sigma_{[CII]}$, of 8.5×10^{40} erg s^{-1} kpc^{-2} and 4.6×10^{40} erg s^{-1} kpc^{-2}.

Although the rest-frame optical photometry of $z > 4$ galaxies can be heavily affected by strong nebular emission lines[39,40], the redshift range $z \approx 6.6$–7.0 offers a unique window where the 4.5 Spitzer/IRAC band is free from contamination by nebular emission lines[7,8], providing a good constraint with which to model the stellar population of galaxies at these redshifts. We used the Bayesian code MAGPHYS[41] with the HIGHZ extension[42] to fit the stellar population. We included the continuum constraints at 243 GHz, but we removed the 3.6-μm Spitzer/IRAC photometry, as this band is affected by high equivalent-width nebular emission ($EW_{[O\,III]+H\beta}$ is about 1,000–1,500 Å; ref. 7). We find that both galaxies have best-fitting stellar masses of about $(1$–$2) \times 10^9 M_\odot$.

Velocity structure and dynamic mass. The line maps extracted in Fig. 1 suggest that the [C II] emission is spatially resolved in both galaxies, which allows us to investigate the presence of any velocity structure in these galaxies. For the central 4″ of the data cube, we extracted a one-dimensional spectrum at every pixel, by averaging all the flux within an elliptical aperture the size of the beam centred on the pixel. We fitted a Gaussian to these spectra, using the parameters from the fit

to the integrated spectrum as initial parameters. We required the fit to the one-dimensional spectrum to be significant at $>5\sigma$.

We measured a projected velocity difference over the galaxies of $111 \pm 28\,\mathrm{km^{-1}}$ and $54 \pm 20\,\mathrm{km^{-1}}$ for COS-3018555981 and COS-2987030247, respectively, using the minimum and maximum central frequencies taken from the fits that are significant at $>5\sigma$. Galaxies with $\Delta v_{\mathrm{obs}}/2\sigma_{\mathrm{tot}}$ ratios greater than 0.4 (using the measured line widths in Extended Data Table 1 to estimate the integrated velocity dispersion) can be classified as probable rotation-dominated systems in cases where the data quality prevents reliable kinematic modelling[25]. This is an approximate diagnostic based on simulations of disk galaxies with a wide range of intrinsic properties. The observed limit of $\Delta v_{\mathrm{obs}}/2\sigma_{\mathrm{tot}}$ at around 0.4 corresponds to the intrinsic ratio of $v_{\mathrm{rot}}/\sigma_0 = 1$ (ref. 25). We tested the robustness of the observed velocity gradient by re-imaging the ALMA data with CASA, using a Briggs weighting with a robustness parameter of 0.5, which produces images of the [C II] emission at a lower signal-to-noise ratio but slightly improved spatial resolution ($0.9'' \times 0.7''$). We confirmed that the same analysis on the higher-resolution data still produced a velocity gradient with the same projected velocity difference over the two galaxies.

We assumed that these galaxies can be described as symmetric rotating disks. This is a reasonable assumption given the consistent prediction of high-resolution hydrodynamic zoom simulations, which show that cool gas indeed settles into regular rotating disks[27,43–45], and given the prevalence of disks among star-forming galaxies at lower redshifts[46–48]. To derive a dynamic mass for these systems, we adopted two methods. First, we use used the approximation that the dynamic mass is estimated from $M_{\mathrm{dyn}}(r < r_{1/2}) = (v_{\mathrm{d}}^2 r_{1/2})/G$, where $r_{1/2}$ is the half-light radius of [C II], G is the gravitational constant, and v_{d} is derived from the average of the observed velocity gradient over the galaxy, $v_{\mathrm{d}}\sin(i) = 1.3\Delta v_{\mathrm{obs}}$ (where i is the disk inclination), and the integrated velocity dispersion, $v_{\mathrm{d}}\sin(i) = 0.99\sigma_{\mathrm{tot}}$ (ref. 25). We estimated a half-light radius ($r_{1/2}$) and the inclination of the system ($\sin(i)$) from an ellipsoidal fit to the [C II] emission line map using CASA (corrected for the beam), and found $r_{1/2}$ values of 2.6 ± 0.8 kpc and 3.1 ± 1.0 kpc, and $\sin(i)$ values of 0.59 ± 0.15 and 0.88 ± 0.06, for our sources. We derived dynamic masses of $(25.3 \pm 15.4) \times 10^9 M_{\odot}$ and $(3.4 \pm 1.7) \times 10^9 M_{\odot}$ for COS-3018555981 and COS-2987030247, respectively.

To obtain a second mass estimate, we modelled the velocity field by assuming that the gas is rotating in a circularly symmetric thin disk, with a gravitational potential that depends only on the disk mass and assuming an exponential distribution of the surface mass density. The circular velocity is projected along the line of sight, weighted by the profile of the intrinsic line surface brightness, and convolved with the beam size of the observations. Free parameters of our model are the inclination of the disk, the position angle of the disk line of nodes, the systemic velocity of the galaxy, and the dynamic mass, measured in a radius of 5 kpc. Our method has been successfully applied to ALMA observations of [C II] emitting sources at redshifts of around 5 (refs 49, 50). Our free parameters were simultaneously constrained from the velocity maps using least-squares fitting. Furthermore, we fitted the coordinates of the disk centre on the basis of the surface brightness maps, which are a minor uncertainty to our final results. We estimated uncertainties from the χ^2 parameter space, which was constrained with Monte Carlo Markov chain simulations. The best-fitting model describes our velocity field well, leaving small residuals (Extended Data Fig. 1). The best-fit parameters indicate half-light radii of $1.7^{+0.4}_{-0.3}$ kpc and $2.1^{+2.1}_{-1.1}$ kpc, inclination angles of $\sin(i) = 0.87^{+0.07}_{-0.10}$ and $0.64^{+0.22}_{-0.30}$, and dynamic masses of $1.0^{+0.3}_{-0.2} \times 10^{10} M_{\odot}$ and $0.4^{+0.9}_{-0.3} \times 10^{10} M_{\odot}$ for COS-3018555981 and COS-2987030247, respectively. These values are all consistent (within the uncertainties) with the estimates derived above. We therefore adopted this more sophisticated method for our fiducial dynamic mass estimates.

In the methods described above, the effect of turbulence on the estimated dynamic masses is not included[51,52]. For dispersion-dominated galaxies, the dynamic mass (including pressure support) can be estimated by $M_{\mathrm{dyn}} = 2R_{1/2}(v_{\mathrm{rot}}^2 + \sigma_0^2)/G$ (ref. 53), where v_{rot} is the inclination-corrected velocity gradient, and we estimate σ_0 values of $55\,\mathrm{km^{-1}}$ and $30\,\mathrm{km^{-1}}$. The resulting dynamical masses are 0.3 dex and 0.4 dex higher than our previous estimates for COS-3018555981 and COS-2987030247, respectively. To study the effect of asymmetric drift on the rotation curve in more detail, higher-resolution observations will be required.

Code availability. The data used here were reduced and partly analysed with the public code CASA, available at https://casa.nrao.edu/casa_obtaining.shtml. The reduction pipeline for this source can be downloaded as part of the ALMA observations with project code 2015.1.01111.S, available in the archive at https://almascience.nrao.edu/alma-data/archive. The kinematic models used for this study are available from the corresponding author upon request.

Data availability. The data used in this publication are publicly available in the data archive https://almascience.nrao.edu/alma-data/archive, and can be retrieved with the project code 2015.1.01111.S or using the name of the principal investigator, 'Smit, Renske'.

31. Chabrier, G. Galactic stellar and substellar initial mass function. *Publ. Astron. Soc. Pac.* **115,** 763–795 (2003).
32. Oke, J. B. & Gunn, J. E. Secondary standard stars for absolute spectrophotometry. *Astrophys. J.* **266,** 713–717 (1983).
33. McMullin, J. P., Waters, B., Schiebel, D., Young, W. & Golap, K. CASA architecture and applications. In *Astronomical Data Analysis Software and Systems XVI* (eds Shaw, R. A., Hill, F. & Bell, D. J.) 127–130 (*Astron. Soc. Pac. Conf. Ser.* Vol. 376, 2007).
34. Dunlop, J. S. *et al.* A deep ALMA image of the Hubble ultra deep field. *Mon. Not. R. Astron. Soc.* **466,** 861–883 (2017).
35. Narayanan, D. *et al.* The IRX-beta dust attenuation relation in cosmological galaxy formation simulations. Preprint at https://arxiv.org/abs/1705.05858 (2017).
36. Koprowski, M. P. *et al.* A resolved map of the infrared excess in a Lyman break galaxy at $z = 3$. *Astrophys. J.* **828,** L21 (2016).
37. Kennicutt, R. C. & Evans, N. J. Star formation in the Milky Way and nearby galaxies. *Annu. Rev. Astron. Astrophys.* **50,** 531–608 (2012).
38. Brammer, G. B. *et al.* 3D-HST: a wide-field grism spectroscopic survey with the Hubble space telescope. *Astrophys. J. Suppl. Ser.* **200,** 13 (2012).
39. Stark, D. P. *et al.* Keck spectroscopy of $3 < z < 7$ faint Lyman break galaxies: the importance of nebular emission in understanding the specific star formation rate and stellar mass density. *Astrophys. J.* **763,** 129 (2013).
40. Smit, R. *et al.* Inferred Hα flux as a star formation rate indicator at $z \sim 4$–5: implications for dust properties, burstiness, and the $z = 4$–8 star formation rate functions. *Astrophys. J.* **833,** 254 (2016).
41. da Cunha, E., Charlot, S. & Elbaz, D. A simple model to interpret the ultraviolet, optical and infrared emission from galaxies. *Mon. Not. R. Astron. Soc.* **388,** 1595–1617 (2008).
42. da Cunha, E. *et al.* An ALMA survey of sub-millimeter galaxies in the extended Chandra deep field south: physical properties derived from ultraviolet-to-radio modeling. *Astrophys. J.* **806,** 110 (2015).
43. Feng, Y. *et al.* The formation of Milky Way-mass disk galaxies in the first 500 million years of a cold dark matter universe. *Astrophys. J.* **808,** L17 (2015).
44. Katz, H., Kimm, T., Sijacki, D. & Haehnelt, M. G. Interpreting ALMA observations of the ISM during the epoch of reionization. *Mon. Not. R. Astron. Soc.* **468,** 4831–4861 (2017).
45. Pallottini, A. *et al.* Zooming on the internal structure of $z \sim 6$ galaxies. *Mon. Not. R. Astron. Soc.* **465,** 2540–2558 (2017).
46. Stott, J. P. *et al.* The KMOS redshift one spectroscopic survey (KROSS): dynamical properties, gas and dark matter fractions of typical $z \sim 1$ star-forming galaxies. *Mon. Not. R. Astron. Soc.* **457,** 1888–1904 (2016).
47. Wuyts, S. *et al.* KMOS3D: dynamical constraints on the mass budget in early star-forming disks. *Astrophys. J.* **831,** 149 (2016).
48. Mason, C. A. *et al.* First results from the KMOS lens-amplified spectroscopic survey (KLASS): kinematics of lensed galaxies at cosmic noon. *Astrophys. J.* **838,** 14 (2017).
49. Carniani, S. *et al.* Strongly star-forming rotating disks in a complex merging system at $z = 4.7$ as revealed by ALMA. *Astron. Astrophys.* **559,** A29 (2013).
50. Williams, R. J. *et al.* Constraining the nature of two Lyα emitters detected by ALMA at $z = 4.7$. *Mon. Not. R. Astron. Soc.* **439,** 2096–2101 (2014).
51. Burkert, A. *et al.* High-redshift star-forming galaxies: angular momentum and baryon fraction, turbulent pressure effects, and the origin of turbulence. *Astrophys. J.* **725,** 2324–2332 (2010).
52. Burkert, A. *et al.* The angular momentum distribution and baryon content of star-forming galaxies at $z \sim 1$–3. *Astrophys. J.* **826,** 214 (2016).
53. Newman, S. F. *et al.* The SINS/zC-SINF survey of $z \sim 2$ galaxy kinematics: the nature of dispersion-dominated galaxies. *Astrophys. J.* **767,** 104 (2013).

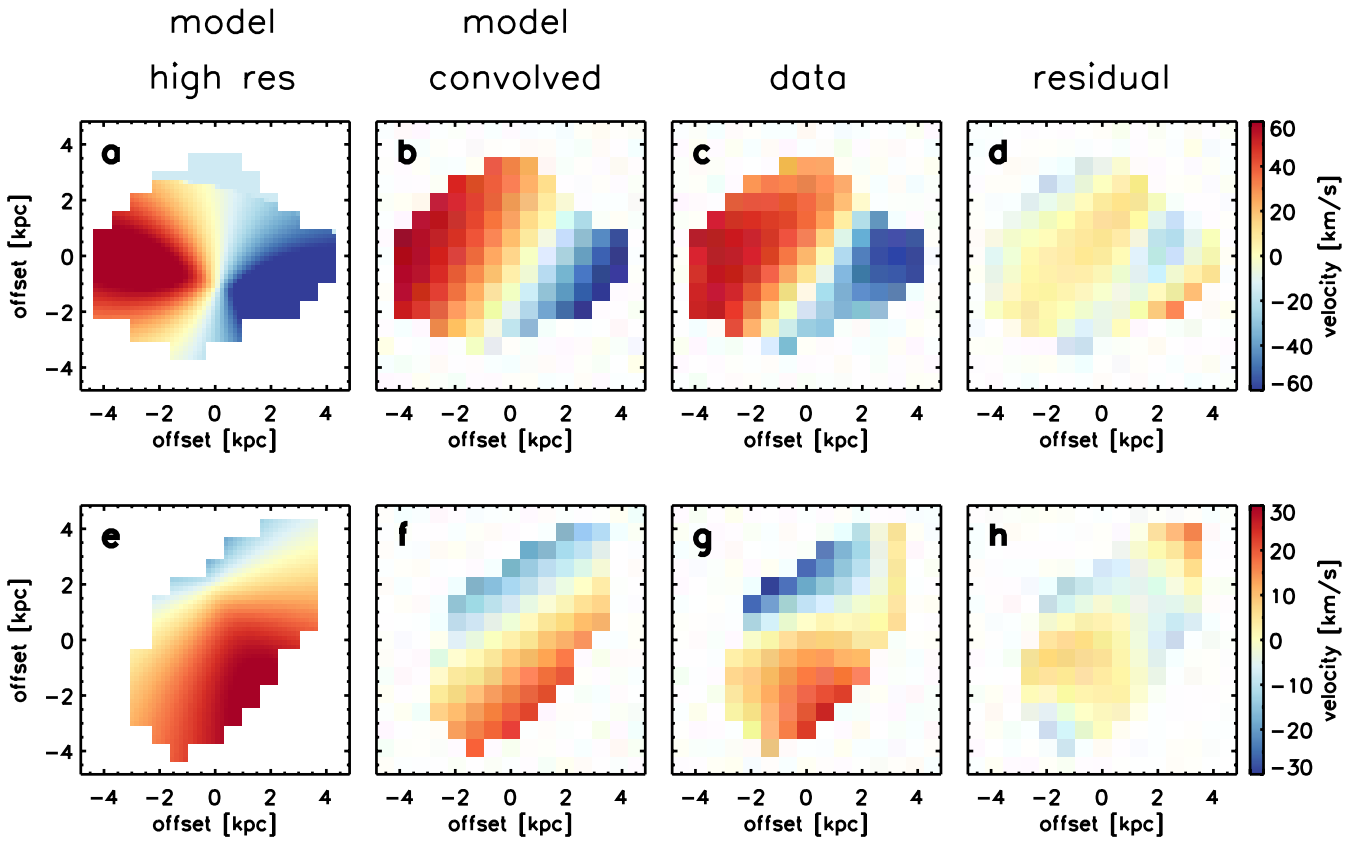

Extended Data Figure 1 | Models of the velocity fields of COS-3018555981 and COS-2987030247, using a disk model. **a**–**h**, Model fits to the velocity gradients in COS-3018555981 (**a**–**d**) and COS-2987030247 (**e**–**h**), assuming that the gas is rotating in an exponential, circularly symmetric thin disk. **a**, **e**, High-resolution disk model before convolution with the beam; **b**, **f**, disk model at the resolution of our observations; **c**, **g**, our velocity maps, as shown in Fig. 3; **d**, **h**, residuals after subtraction of the model. Although the disk model is not a unique solution for these velocity fields, our galaxies are well described by regular rotation.

Extended Data Table 1 | Galaxy properties

ID	COS-3018555981	COS-2987030247
z_{phot}[7]	6.76±0.07	6.66±0.14
$z_{[CII]}$*	6.8540±0.0003	6.8076±0.0002
S/N†	8.2	5.1
[C II] line flux (Jy km s^{-1})*	0.39±0.05	0.31±0.04
FWHM$_{[CII]}$ (km s^{-1})*	232±30	124±18
158μm continuum flux (μJy)	<87‡	<75‡
$L_{[CII]}$ (10^8 $L_\odot$)	4.7±0.5	3.6±0.5
L_{UV} (10^{11} $L_\odot$)	1.1±0.1	1.3±0.1
L_{IR} (10^{11} $L_\odot$)	<1.3‡	<1.1‡
SFR$_{IR}$ ($M_\odot$ yr^{-1})	<19‡	<16‡
SFR$_{UV}$ ($M_\odot$ yr^{-1})	19.2±1.6	22.7±2.0
M_* (10^9 $M_\odot$)	$1.4^{+0.7}_{-0.2}$	$1.7^{+0.5}_{-0.2}$
M_{dyn} (10^9 $M_\odot$)	10^{+3}_{-2}	4^{+9}_{-3}
Δv_{obs} / $2\sigma_{tot}$	0.57±0.16	0.52±0.21
$r_{1/2,[CII]}$ (kpc)	2.6±0.8	3.1±1.0
β_{UV}	−1.22±0.51	−1.18±0.53
EW([O III]+Hβ) (Å)[7]	1424±143	1128±166

*These values were measured from a Gaussian fit to the integrated spectrum within the half-peak-power contour.
†The signal-to-noise ratio (S/N) was measured in a beam-sized aperture (centred on the HST counterpart) on a velocity-averaged image extracted over the detected line.
‡3σ limit.